ELSEVIER

Journal of Hazardous Materials B133 (2006) 218–225

Journal of Hazardous Materials

www.elsevier.com/locate/jhazmat

Combined effect of Bond and capillary numbers on hydrocarbon mobility in water saturated porous media

Francesco Gioia *, Massimo Urciuolo

Dipartimento di Ingegneria Chimica, Università di Napoli Federico II, Piazzale Tecchio, 80125 Napoli, Italy

Received 7 March 2005; received in revised form 6 October 2005; accepted 7 October 2005
Available online 15 December 2005

Abstract

The mobilization of an oil bank under the combined effect of Bond ($\mathbf{N}_B$) and capillary ($\mathbf{N}_C$) numbers, in a packed bed column of glass beads saturated with water, has been investigated. In order to reach the irreducible saturation the experiments have been run with sweeping water velocities outside the range of validity of the Darcy's law. The size of the glass beads was varied in the range between 2 mm and 5 mm. The oils used for the tests are hexadecane and hexane with viscosities different for an order of magnitude and densities smaller than that of water, and α-methylnaphthalene, which has a density very close to that of water, in order to single out the effect of the capillary number on the mobilization process. The plots of oil saturation as function of the trapping number ($\mathbf{N}_T$), which is the vectorial sum of $\mathbf{N}_B$ and $\mathbf{N}_C$, are reported and a mobilization diagram is drawn. Furthermore, a few tests in a basin, simulating an aquifer at a laboratory scale, have proved that the results obtained in the packed column are useful for determining the fate of a spill of oil above an aquifer. For these experiments also perchloroethylene (PCE), which has a density greater than that of water, has been used.

Keywords: Capillary number; Bond number; LNAPL/DNAPL mobility in aquifer

1. Introduction

The flow through water saturated granular porous media of a dispersed immiscible phase is of great practical interest in connection with underground-water pollution by organic solvents and other petroleum derived products, which may enter the subsurface. Many papers, with quite different approaches to the study of this multifaceted problem, have been published. Ng and Payatakes [1], Payatakes et al. [2], Dias and Payatakes [3] and Avraam and Payatakes [4] aim at obtaining a macroscopic description of the mobilization and break up phenomenology focusing the attention on the microscopic mechanism of the two-phase flow. Other authors (Powers et al. [5] and Mayer and Miller [6,7]) by setting up properly designed experiments, focus the attention on the characterization of the ganglia size distribution in unconsolidated porous media as a function of the particle size. Pennel et al. [8], in order to investigate on the mobilization of a dispersed phase during surfactant flushing, perform column experiments in unconsolidated porous media (Ottawa sand). An interesting theoretical and experimental investigation for describing the interplay of capillary, viscous and buoyancy forces in the mobilization of a single oil blob is provided by Morrow [9]. The porous medium is simulated by a simple model obtained by packing equal spheres (radius 0.125 in.) in cubic array. A further comprehensive experimental investigation for determining the capillary number relationships for displacement of both residual and initially continuous oil from various water-wet consolidated sandstones is provided by Chatzis and Morrow [10]. In this last paper, the attention is focused mainly on the oil displacement, down to a 50% residual saturation, while the water velocity is kept in the range of validity of Darcy's law. No information is given explicitly on the role played by the Bond number. In the present paper, the investigation is extended to the study of the mobilization, down to the irreducible saturation, of a variety of dispersed oils in unconsolidated water saturated porous media. In order to attain the irreducible saturation the experiments have been done with sweeping water velocities outside the range of validity of the Darcy's law. The interplay of both the Bond and the capillary numbers is investigated.

* Corresponding author. Tel.: +39 081 7682277; fax: +39 081 2391800.
E-mail address: gioia@unina.it (F. Gioia).

0304-3894/$ – see front matter © 2005 Elsevier B.V. All rights reserved.
doi:10.1016/j.jhazmat.2005.10.010

Nomenclature

D	diameter of the column (cm)
D_p	diameter of a glass bead (cm)
DSS	dioctyl sulfosuccinate sodium salt (surfactant)
h_{aq}	height of the aquifer (cm)
Hed	hexadecane
Hex	hexane
k	intrinsic permeability of the porous bed (cm^2)
$\mathbf{k}$	unit vector opposite to gravity (pointing upward)
k_{rw}	relative permeability to the aqueous phase
L	height of the packing (cm)
$\mathbf{N}_B$	Bond number (see Eq. (1))
$\mathbf{N}_C$	capillary number (see Eq. (2))
$\mathbf{N}_T$	trapping number, $\mathbf{N}_B + \mathbf{N}_C$
PCE	perchloroethylene (tetrachloroethylene)
Q	water flow rate (cm^3/s)
Re	Reynolds number $(D_p \rho v_o/\mu_w)(1-\varepsilon)^{-1}$
S	cross-sectional area of the column (cm^2)
S_{ir}	irreducible saturation (%)
S_{oil}	oil saturation (%)
$\mathbf{v}_o$	superficial velocity ($v_o = Q/S$) (cm/s)
$(v_o)_{max}$	velocity at which the irreducible saturation is reached (cm/s)
V_{oil}	volume of oil present in the column (cm^3)
V^o_{oil}	volume of oil injected (cm^3)

Greek letters

α-MN	α-methylnaphthalene
$\boldsymbol{\delta}_i$	unit vector
$\Delta\rho$	is $\rho_w - \rho_o$ (g/cm^3)
$\Delta\mathcal{P}$	pressure drop ($dyne/cm^2$)
ε	porosity of the bed in the absence of oil
ε'	porosity in the presence of oil at any v_o
ε'_o	initial porosity in the presence of the volume V^o_{oil} of oil
μ	viscosity of the oil ($g\,cm^{-1}\,s^{-1}$)
μ_w	viscosity of water ($g\,cm^{-1}\,s^{-1}$)
ρ_m	density of α-methylnaphthalene (g/cm^3)
ρ_o	density of oil phase (g/cm^3)
ρ_w	density of water (g/cm^3)
σ_{ow}	interfacial tension between the oil and the aqueous phase (dyne/cm)
·	scalar product

The problem of flushing with water a discontinuous oil phase from a porous medium, is quite complex inasmuch as many physical phenomena are simultaneously involved, e.g. the geometry and the local structure of the porous medium, the dynamics of fluids in porous media, the capillary phenomena and the physical properties of the oil (viscosity, density, interfacial tension, etc.). The main purpose of our work was to focus the attention on the role played by the capillary retention forces and by the dynamics of water flow on the mobilization of the dispersed oil. In order to reduce the overall complexity of the problem, the study has been carried out reducing to the minimum the uncertainties related to the local geometry of the porous structure. To this purpose, the experiments have been performed in a plexiglas column filled with uniformly sized spherical glass beads. For such system, which has a well-known geometry and local porosity structure, the dynamics of water flow can be modeled with good accuracy and reliable fluid flow models are available in the literature; so that the role played by the oil properties could be confidently singled out and investigated. Furthermore, the transparency of the experimental set-up was of a great help for observing (and camera recording) the phenomenology of mobilization and fragmentation.

In a previous paper [11], we have focused the attention on the oil in a porous medium saturated with stagnant water, in order to study the influence of buoyancy force on the mobilization of the oily phase. Under such condition, the mobilization depends on the value of the Bond number only. The experimental results showed that a bank of oil for which the N_B is below the critical value (i.e. 2×10^{-3}), shows an initial mobility due to fingers that move along preferential patterns. Eventually, these fingers break up in smaller ganglia and/or droplets (with a size comparable to that of the solid particles), which remain immobile in the interstices of the porous medium. For values of $N_B > 8 \times 10^{-3}$, the ganglia generated from the bank definitely move, undergoing stranding and successive fragmentation, "dynamic break up", and the oil, depending on the sign of $\Delta\rho$, eventually reaches the top or the bottom of the porous medium. Even the smallest droplets, in their majority, leave the medium. Only the irreducible saturation is left in the porous medium. For $2 \times 10^{-3} < N_B < 8 \times 10^{-3}$, an intermediate situation is observed (partial mobility). For this case only the large ganglia move and undergo fragmentation, generating smaller ganglia entrapped in the porous medium.

In the present paper, we have carried on experiments in order to find an analogous correlation of mobilization of an oily phase in water versus the value of the capillary number $\mathbf{N}_C$. The results of these experiments permit to gain an insight on the fate of an oil spill which reaches the aquifer.

2. Theory

The movement of an oil ganglion in a saturated porous material is regulated by two dimensionless numbers: Bond number and capillary number. They are defined here as:

$$\mathbf{N}_B = \frac{k k_{rw}\,\Delta\rho g}{\sigma_{ow}}\mathbf{k} \tag{1}$$

$$\mathbf{N}_C = \frac{\mu_w \mathbf{v}_o}{\sigma_{ow}} \tag{2}$$

The two numbers represent the ratio of buoyancy force and of shear stress to the capillary retention force, respectively. It must be remarked that they have a vectorial character. $\mathbf{N}_B$ is directed as the gravity and points up or down according to the sign of $\Delta\rho$. $\mathbf{N}_C$ is directed and points as the velocity $\mathbf{v}_o$ in the porous medium. Therefore, $\mathbf{N}_B$ and $\mathbf{N}_C$ combine their effect on the mobility of a

ganglion of oil as a vector, which in orthogonal coordinates is:

$$\mathbf{N}_B + \mathbf{N}_C = \sum_i \boldsymbol{\delta}_i (N_{B_i} + N_{C_i}); \quad i = 1\text{–}3 \tag{3}$$

where $\boldsymbol{\delta}_i$ are the "unit vectors" in the direction of the 1–3 axes. The magnitude of this vector is:

$$|\mathbf{N}_B + \mathbf{N}_C| = \sqrt{\sum_i (N_{B_i} + N_{C_i})^2} \tag{4}$$

For the case of Cartesian coordinates the axes 1, 2, 3 correspond to the usual notation of x, y, z, and the unit vectors are called **i**, **j**, **k**.

In a stagnant fluid it exists a critical value of $|\mathbf{N}_B|$ say N_{Bc} below which the capillary retention force is larger than the buoyancy force so that the ganglion remains immobile when subject to gravity only. In a previous paper [11], we have determined the range of N_B values for which oil ganglia remain immobile in unconsolidated porous media saturated with a stagnant aqueous phase. It is the purpose of this paper to find the analogous range for the capillary number.

Say N_{Cc} the critical value of $|\mathbf{N}_C|$ below which the shear stress does not overcome the capillary retention force. Naturally, N_{Cc} cannot be independently measured because the buoyancy force is always present. Rather, the combination $|\mathbf{N}_B + \mathbf{N}_C|_c$ would be measured in any experiment. Following Pennel et al. [8], we define $\mathbf{N}_B + \mathbf{N}_C$ as the trapping number $\mathbf{N}_T$. Assume that an experiment is made for which gravity and the water velocity have the same direction z, in such case the immobility condition for an oil ganglion is:

$$N_T < N_{Bc} \pm N_{Cc} = N_{Tc} \tag{5}$$

The negative sign applies when $\mathbf{N}_C$ and $\mathbf{N}_B$ are opposite vectors.

3. Experimental

The experiments described in this section are aimed at determining the mobilization induced by the shear stress due to the water velocity: namely mobilization versus N_C. Two sets of experiments were arranged. The first set was carried out in a vertical plexiglas column. In this case, $\mathbf{N}_B$ and $\mathbf{N}_C$ have the same direction. The second set was made in a plexiglas basin simulating an aquifer. In this case, $\mathbf{N}_B$ and $\mathbf{N}_C$ are about orthogonal.

3.1. Experiments in the column

The assembly for running these experiments is sketched in Fig. 1. The plexiglas column (4.1 cm internal diameter) was filled with uniformly sized glass beads for a height of 44 cm and saturated with water. Three sizes of beads were used; i.e. 2 mm, 3 mm and 5 mm. The water was fed by a gear pump (Verder Lab Tech GmbH, model VG 1000 digit) with interchangeable heads for covering a water flow rate in a large range; up to 4000 ml/min. The flow rate was measured by means of one of three rotameters according to the value of the flow rate to be measured. They were

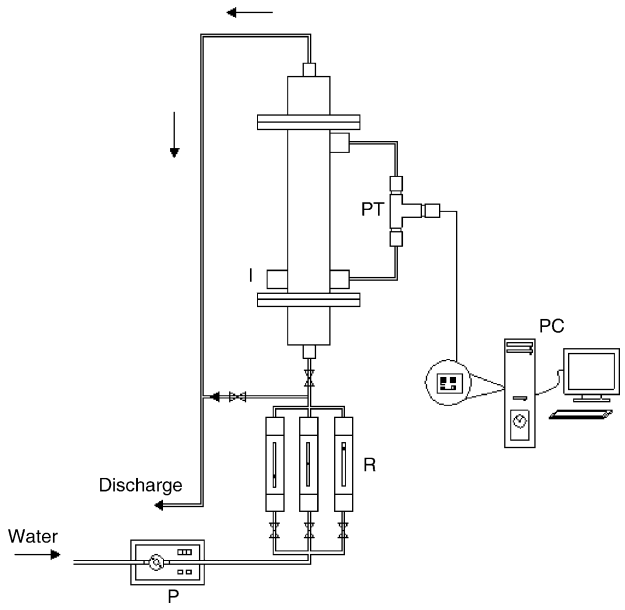

Fig. 1. Experimental set-up of packed column—P: gear pump with interchangeable heads for different flow rate ranges; R: rotameters for different flow rate ranges; PT: pressure transducer; PC: personal computer equipped with data logger and Labview software; I: injection port for oil.

accurately calibrated using graduated containers and a stopwatch. Pressure drop across the bed was measured by a pressure transducer (Druck PMP4000 series, range 0–70 mbar ± 0.04% F.S.) and recorded by a PC equipped with a data logger (National Instruments PCI-6034E with National Instruments Labview 5.1 software).

The oils used in the experiments are: hexane, hexadecane and α-methylnaphthalene. The first two have a density smaller than that of water. Thus, for both of them it is $\mathbf{N}_B \cdot \mathbf{k} = N_B > 0$. For α-methylnaphthalene, because $\rho_m \approx \rho_w$, it is $N_B \approx 0$ and the mobility is regulated about exclusively by the capillary number. The properties of the oils and of the porous medium are reported in Tables 1 and 2, respectively. The oil/water interfacial tension was measured by an Optical Contact Angle Meter tensiometer

Table 1
Relevant properties of the oils

Oil	ρ (g/cm^3)	μ (cP)	σ_{ow} (dyne/cm)
Hex	0.659	0.29	38.7
Hed	0.774	2.89	38.8
α-MN	1.009	1.77	47.6
PCE	1.632	0.88	36.5

Hed, *n*-hexadecane; Hex, *n*-hexane; α-MN, α-methylnaphthalene; PCE, perchloroethylene (tetrachloroethylene).

Table 2
Property of the glass bead packed column

D_p (mm)	ε	k (Eq. (12)) (cm^2)
5	0.408	3.25×10^{-4}
3	0.386	9.13×10^{-5}
2	0.379	3.76×10^{-5}

The porosity is measured by the dynamic method.

Table 3
Operating conditions of the experiments

Run	D_p (mm)	Oil	V^o_{oil} (cm^3)	S_{ir} (%)	N_B at 20 °C	$(v_o)_{max}$ (cm/s)	$(N_C)_{max}$	$(N_T)_{max}$	Re_{min}
1	5	α-MN	16.0	0.586	-2.18×10^{-4}	4.9	1.02×10^{-3}	8.2×10^{-4}	44
2	5	Hed	20	0.3	1.67×10^{-3}	4.6	1.19×10^{-3}	3.0×10^{-3}	44
3	5	Hex	20	0.036	2.62×10^{-3}	4.8	1.25×10^{-3}	3.9×10^{-3}	44
4	3	Hed	20	0.103	4.69×10^{-4}	4.8	1.24×10^{-3}	1.8×10^{-3}	42
5	3	Hex	20	0.073	7.36×10^{-4}	4.8	1.25×10^{-3}	2.1×10^{-3}	42
6	3	α-MN	16.2	0.284	-5.34×10^{-5}	4.8	1.02×10^{-3}	9.2×10^{-4}	42
7	2	Hed	18.5	0.435	1.93×10^{-4}	4.8	1.24×10^{-3}	1.7×10^{-3}	42
8	2	α-MN	12.2	0.008	-2.48×10^{-5}	4.7	1.01×10^{-3}	1.1×10^{-3}	42

$(v_o)_{max}$ and $(N_C)_{max}$ are the superficial velocity and the capillary number when the irreducible saturation is reached. S_{ir} as calculated by Eq. (11).

(CAM 200, KSV Instruments Ltd.). The oil, was red coloured by adding about 1% weight of a die immiscible with water. The addition of the die did not alter significantly the oil/water interfacial tension. The details of the operating conditions of the experiments are reported in Table 3.

A volume V^o_{oil} of coloured oil was injected by a syringe through the injection port at the bottom of the packed column in the absence of a flux of water. When the oil dispersion in the column was stabilized, water was fed at the bottom of the column by the volumetric pump and the flow rate was slowly increased and recorded together with the pressure drop versus time. The evolution of the oily phase was followed by a digital video camera.

In order to single out the influence of N_C alone on the mobilization process, we carried out runs 1, 6 and 8 with α-methylnaphthalene, which has a density very close to that of water ($N_B \approx 0$). After the injection this compound remains at the bottom of the column as a continuous phase. Namely as a bank filling completely the porosity.

The experiments have explored a quite large range of water flow rate. In fact, the flow rate Q has been varied in the range 3–230 l/h, correspondingly the superficial velocity v_o is in the range 0.065–5 cm/s and the Reynolds number is in the range: $Re_{min} = 42$; $Re_{max} = 3390$.

3.2. Oil saturation versus trapping number

The porosity of the bed was determined according to two different methods. In the first (static method), the beads were loaded in a graduate cylinder (same diameter as the column) and their apparent volume V_a was recorded. The bed was then saturated with water whose volume V_w was recorded too. By definition it is $\varepsilon = V_w/V_a$. The second is a dynamic evaluation of the porosity made directly in the column. A measured flow rate of water was fed at the bottom of the column in which the dry beads were packed. The time t taken by the front of the water to sweep a measured height of the column was recorded. The dynamic porosity is the ratio between the volume of water fed in the time t divided the volume of column swept by the front of water in the same time t. The results are comparable with those obtained by the static measurement described above. However, we will use the dynamic porosity values as they are directly measured in the column.

The measured porosities for the three sizes of beads used in the experiments are reported in Fig. 2. Theoretically, the porosity for spherical glass beads should not change with the size of the beads. However, inspection of Fig. 2 shows that ε increases as the diameter of the beads increases. This is due to a wall effect. Close to the wall the porosity is larger than in the core of the column. This effect plays a role relatively bigger as the ratio D_p/D increases. Mehta and Hawley [12] have proposed a model to describe the porosity in a packed bed taking into account the wall effect. It is:

$$\varepsilon = 0.3517 + 0.4657\frac{D_p}{D} \tag{6}$$

The value 0.3517 is the extrapolation to $D_p/D \to 0$ of the data in Fig. 2. All the experiments we have carried out, even for the smallest flow rate are for $Re > 10$ (see Table 3). In this instance, Darcy's law is not applicable and the pressure drop across a packed bed is described by Ergun's equation [13] modified by Mehta and Hawley [12] to include the wall effect. This equation however is more and more accurate as $D_p/D \to 0$, namely when ε is uniform in the whole bed. For the case at hand, due to the wall effect, according to [12] a modified form of the Ergun equation must be used. It is:

$$\frac{-\Delta\mathcal{P}}{L} = \frac{150\mu v_o}{D_p^2}\frac{(1-\varepsilon)^2}{\varepsilon^3}M^2 + \frac{1.75\rho v_o^2}{D_p}\frac{1-\varepsilon}{\varepsilon^3}M \tag{7}$$

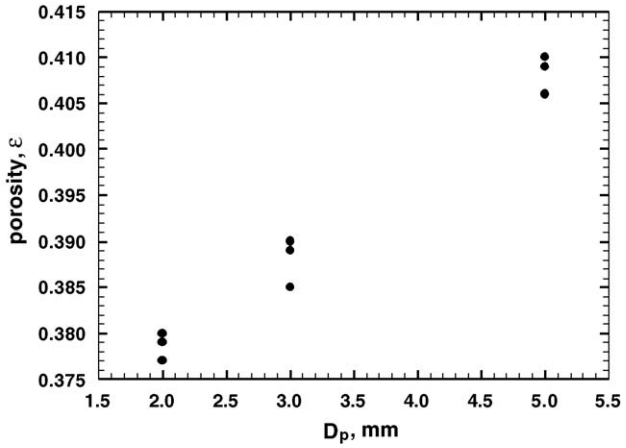

Fig. 2. Porosity of the packed bed vs. the diameter of the beads loaded.

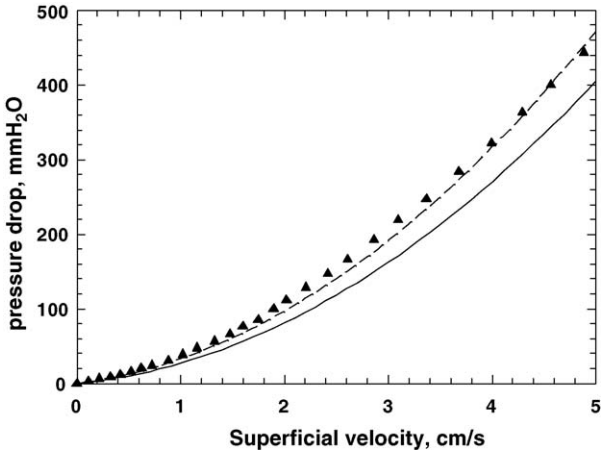

Fig. 3. Measured pressure drop data across the column vs. v_o for 5 mm beads. Continuous line: Ergun equation; short dash line: Eq. (7).

where M is a correction factor for the wall effect; i.e.:

$$M = 1 + \frac{4D_p}{6D(1-\varepsilon)} \tag{8}$$

Fig. 3 shows the great accuracy of Eq. (7) for fitting the measured pressure drop versus the superficial velocity (with no oil in the column), as compared to the classical Ergun's equation. The comparison is for the largest particle diameter used in our experiment: $D_p = 0.5$ cm for which the wall effect is largest. Eq. (7) is the tool that will be used in the following for constructing a mobility diagram of oils versus the trapping number.

As an example, with reference to run 4, we describe, step by step, the procedure for constructing the mobilization diagram. Firstly, the pressure drop in the absence and in the presence of the oil (hexadecane) is measured and plotted versus the water velocity as in Fig. 4. The porosity ε in the absence of oil is 0.386 (from Fig. 2). Upon the addition of the oil the initial void volume is reduced for the volume of the oil. Therefore, the new porosity which is the ratio of the actual void volume to the volume of the column becomes:

$$\varepsilon'_o = \varepsilon - \frac{V^o_{oil}}{SL} \tag{9}$$

It is $\varepsilon'_o = 0.351$. Then, the theoretical pressure drop versus the superficial velocity v_o both in the absence and in the presence of oil is calculated by means of Eq. (7) using ε and ε'_o, respectively. The two curves are reported in Fig. 4. Inspection of this figure shows that the two theoretical curves diverge while the experimental data first diverge but as the flow rate increases further they converge and join at $(v_o)_{max} = 4.8$ cm/s. This behaviour is consistent with the observation that as the water velocity is increased the oil at a velocity corresponding to point A (Fig. 4) begins to leave the column, and at $v_o = 4.8$ cm/s only the irreducible saturation (about 0% of oil) is eventually left in the column, and it becomes $\varepsilon \approx \varepsilon'$. The percent of the oil loaded present in the column at any velocity is calculated as follows. By means of Eq. (7), given $\Delta\mathcal{P}$ and v_o, the porosity ε' is determined and the percent of oil remaining in the column at any v_o is:

$$\%\text{Oil} = \frac{V_{oil}}{V^o_{oil}} \times 100 = \frac{SL(\varepsilon - \varepsilon')}{V^o_{oil}} \times 100 \tag{10}$$

The percent saturation of oil (i.e. the percent of oil present in the porosity at any v_o) is:

$$S_{oil} = \left(\frac{\varepsilon}{\varepsilon'} - 1\right) \times 100 \tag{11}$$

The above calculations have been carried out for all ranges of v_o and repeated for all runs. The diagrams S_{oil} versus the trapping number are reported in Fig. 5. Notice that the curves fall in different ranges of the trapping number as different oils show different values of both the Bond and the capillary numbers.

The intrinsic permeability, which enters the Bond number (Eq. (1)), has been calculated by means of the equation:

$$k = \frac{D_p^2}{150}\frac{\varepsilon^3}{(1-\varepsilon)^2} \tag{12}$$

The relative permeability to the water phase k_{rw} tends to unity as the saturation tends to zero. In our experiments, the oil

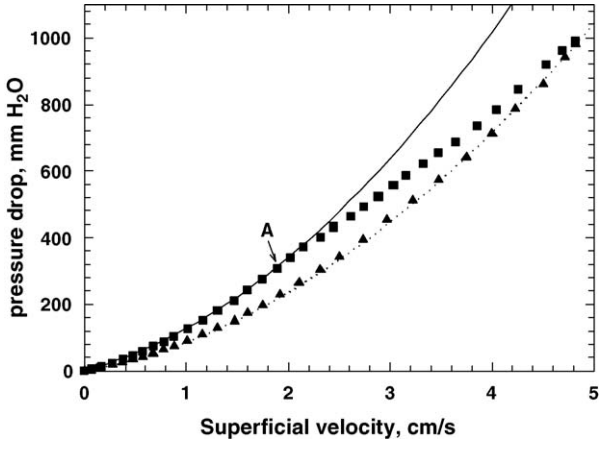

Fig. 4. Pressure drop across the column vs. v_o in the absence of oil (▲), in the presence of hexadecane (■) for 3 mm beads. The curves are—continuous line: Eq. (7) with ε'_o; dotted line: Eq. (7) with ε (run 4 of Table 3).

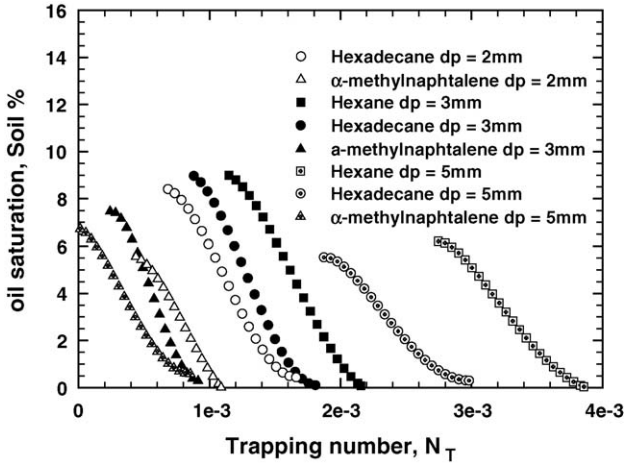

Fig. 5. Percent oil saturation vs. the trapping number for all runs.

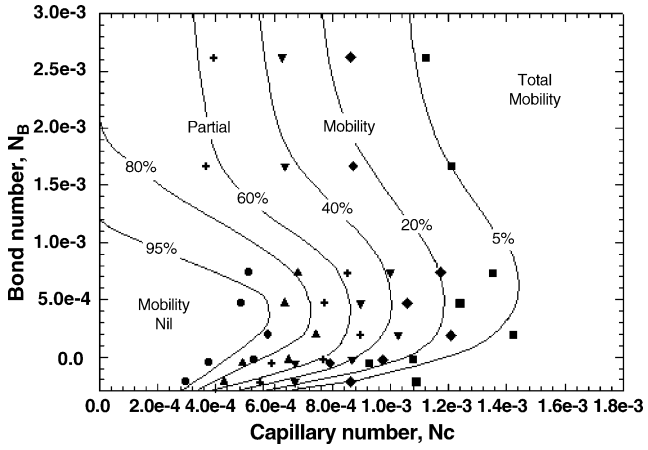

Fig. 6. Mobility diagram with data points. The residual oil saturations are: (●) 95%, (▲) 80%, (✚) 60%, (▼) 40%, (♦) 20% and (■) 5%. Symbols for the same N_B (see Table 3) are for a given oil but different bead size.

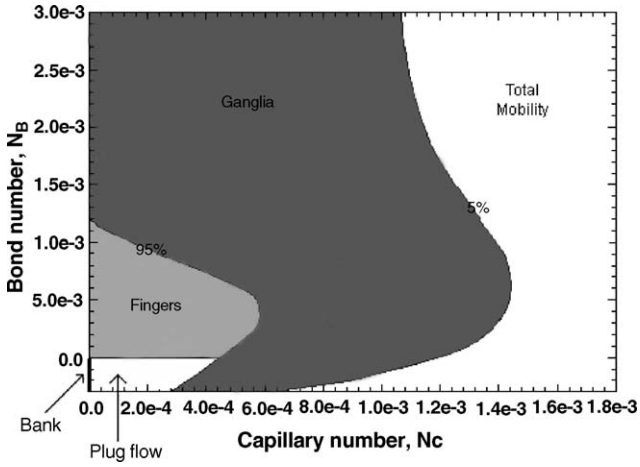

Fig. 7. Sketch of the mobility diagram.

is largely dispersed in the column; therefore, it can be set $k_{rw} = 1$.

3.3. Mobility diagram

Having determined the oil saturation curves, it is possible to draw the mobility diagram in Fig. 6. It is a diagram which has the Bond number on the *y*-axis and the capillary number on the *x*-axis. The data points of iso-percent of oil present in the column are acquired from the oil saturation curves (e.g. Fig. 5). Given the oil and the bead diameter, N_B is calculated and N_C is determined at various percent of oil for the given N_B value, from the oil saturation diagrams. The iso-percent curves in Fig. 6 are hand drawn. The initial points of these curves at $N_C = 0$ are obtained from Gioia et al. [11]. In the same diagram the ranges of the mobility condition of the oil are indicated. The detail of calculations is reported in [14]. The residual saturations, which cannot be easily read in the diagrams of Figs. 5 and 6, are reported in Table 3.

Inspection of Fig. 6 shows that for $N_B < 1.2 \times 10^{-3}$ and $N_C = 0$ a mobility nil is observed (more than 95% of the oil loaded remains in the column). In the range $1.2 \times 10^{-3} < N_B < 8 \times 10^{-3}$, a partial mobilization occurs [11]. On the contrary, with reference to the runs with α-methylnaphthalene, for $N_B \approx 0$ (because $\rho_w - \rho_m \approx -0.009$ g/ml N_B is not truly nil but slightly smaller than zero; all data points at $N_B < 0$ are obtained with α-methylnaphthalene), a partial mobilization starts at N_C around 2×10^{-4}, and a total mobilization at N_C of the order of 7×10^{-4}. In conclusion, in our experiments it is: $N_{Cc} \approx 2 \times 10^{-4}$ and $N_{Bc} \approx 10^{-3}$. Namely the numerical value of the capillary number, which induces mobilization is about an order of magnitude less than the Bond value which would produce the same mobilization. These results are consistent with those by Chatzis and Morrow [10] considering, however, that these authors have worked with porous sandstones with a much lower porosity. The mobility diagram has been redrawn in a more readable form in Fig. 7. The presence of negative values of N_B did not permit to draw the diagram in log scale.

3.4. Experiments in the basin

A sketch of this apparatus is reported in Fig. 8. At the bottom of the case, a layer about 6 cm thick of beads of desired size was spread. The thickness was such that the upper surface of the bed was a few centimeters above the water table. The layer was covered (covering soil) with dry beads 0.5 mm diameter for a height of 9 cm. A water flow was started and measured, when the flow rate was stabilized a volume of oil was spilled on the top of the dry beads and quickly (being the covering soil dry) reached the capillary fringe. In the real case, however, the solid may be humid and the descent of the oil slowed by the capillary retention forces. The oils used are hexadecane (lighter than water), and perchloroethylene (PCE; heavier than water) as a representative of chlorinated solvents commonly found at DNAPL contaminated sites. The operating conditions of these runs are in Table 4. Details on the experimental procedure are reported in [15].

For runs 1 and 2, the scalar product $\mathbf{N_B} \cdot \mathbf{k} > 0$ (oil lighter than water) the oil sets on the capillary fringe without penetrating into the aquifer. Furthermore, being $|\mathbf{N_C}| < N_{Cc}$ the oil does not move along the direction (horizontal) of flow in the aquifer and the contamination of the water downstream is essentially due to

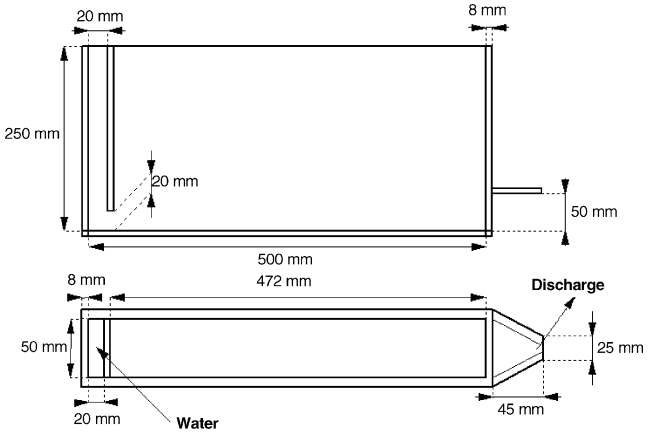

Fig. 8. Experimental set-up of the basin for simulating an aquifer.

Table 4
Runs in the basin simulating an aquifer

Run	D_p (mm)	h_{aq} (cm)	Oil	Aqueous phase	σ_{ow} (dyne/cm)	ε[a]	k (Eq. (12)) (cm^2)	N_B	v_o (cm/s)	N_C	Mobility condition
1	2	5.2	Hed	Water	39.4	0.41	5.3×10^{-5}	3.0×10^{-4}	0.014	3.5×10^{-6}	i.
2	5	5.0	Hed	Water	39.4	0.43	4.1×10^{-4}	2.3×10^{-3}	0.014	3.5×10^{-6}	p.m.
3	2	6.8	PCE	Water	36.5	0.41	5.3×10^{-5}	-9.0×10^{-4}	0.11	3.0×10^{-5}	i.
4	5	5.5	PCE	Water	36.5	0.43	4.1×10^{-4}	-7.0×10^{-3}	0.10	2.7×10^{-5}	p.m.
5	5	5.2	PCE	W + DSS[b]	0.2	0.43	4.1×10^{-4}	-1.27	0.10	5.0×10^{-3}	t.m.

p.m.: partial mobility with N_B; t.m.: total mobility; i.: immobile.
[a] ε is measured by the static method.
[b] Water + DSS, 1.2 wt.%.

the solubilization of the oil. The oil forms a floating bank on the top of the aquifer vertically below the point where the spill occurred (if the covering soil is isotrope). In this instance, there is a reasonable hint on where to create a well for aspirating the oil. Even vertical oscillations of the aquifer level that we created on purpose, will not mobilize the oil bank.

For runs 3 and 4, tetrachloroethylene (PCE) was used as the non-aqueous phase. For these runs, $\mathbf{N_B}\cdot\mathbf{k} < 0$ (oil heavier than water) therefore the oil could migrate downwards through the aquifer. However, being $|\mathbf{N_B}| \leq N_{Bc}$, the oil does not massively migrate, but distributes as ganglia and droplets in the porosity of the aquifer. The water flow, even though we achieved water velocities much larger than typical values in aquifers, being $|\mathbf{N_C}| < N_{Cc}$ did not mobilize the PCE which remained immobile in the porosity of the aquifer. In all previous cases, with the superficial velocity accessible in the apparatus, it was $Re < 10$ and we never reached values $N_C > N_{Cc}$. In order to force N_C to be larger than N_{Cc} we had to reduce the interfacial tension by adding a surfactant to the water. In particular, run 5 was done adding to water dioctyl sodium sulfosuccinate at 1.2 wt.% ($\sigma_{ow} \approx 0.2$ dyne/cm) so that it was $|\mathbf{N_C}| > N_{Cc}$. In this case, the oil quickly moved downwards and reached the right corner at the bottom of the basin.

4. Conclusions

The experimental results permit to determine the mobility condition of a bank of oil infused in an unconsolidated porous material, saturated with an aqueous phase. In particular, it has been determined the range of values of both N_B and N_C for which the mobility of oil is observed.

With still water if $|\mathbf{N_B}| > 8 \times 10^{-3}$ a bank of oil (LNAPL) injected at the bottom of the porous medium will undergo a "dynamic break up" generating ganglia which go through stranding and successive fragmentation and will move toward the top until all the oil has left the porous bed. Even the smaller droplets, in their majority, reach the top of the column. If $|\mathbf{N_B}| < 1.2 \times 10^{-3}$ the bank will show an initial mobility due to fingers that move along preferential patterns. Eventually, these fingers break up in smaller ganglia and/or droplets (with a size comparable to that of the particles), which will remain entrapped in the interstices of the porous bed. For $1.2 \times 10^{-3} < |\mathbf{N_B}| < 8 \times 10^{-3}$, a partial mobility is predicted. Only part of the oil (the larger ganglia) will exit the porous medium, even though undergoing fragmentation, generating smaller ganglia and/or droplets, which remain entrapped in the porous bed. For this case, only part of the oil leaves the bed.

In the presence of a flow of water, the mobility of the oil is regulated by the vectorial sum of $\mathbf{N_B}$ and $\mathbf{N_C}$, which is defined as the trapping number.

A few runs using α-methylnaphthalene (for which $N_B \approx 0$) have permitted to study the effect of N_C alone and to determine the minimum value of N_C ($N_{Cc} = 2 \times 10^{-4}$) above which a mobility of the oil is observed. The results of the experiments have allowed us to draw a diagram which permits to establish at a glance the mobility conditions of a bank of oil in dependence of the values of the N_B and N_C numbers.

Finally, a few experiments in a basin, simulating at a laboratory scale an aquifer, have proved that the results obtained in the packed column are useful for determining the fate of a spill of oil above an aquifer.

Acknowledgment

This work was financed by "Dipartimento della Protezione Civile—Gruppo Nazionale per la Difesa dai Rischi Chimico-Industriali ed Ecologici del Consiglio Nazionale delle Ricerche".

References

[1] K.M. Ng, A.C. Payatakes, Stochastic simulation of the motion, breakup and stranding of oil ganglia in water-wet granular porous media during immiscible displacement, AIChE J. 26 (1980) 419–428.
[2] A.C. Payatakes, K.M. Ng, R.W. Flumerfelt, Oil ganglion dynamics during immiscible displacement: model formulation, AIChE J. 26 (1980) 430–443.
[3] M.M. Dias, A.C. Payatakes, Network models for two-phase flow in porous media, J. Fluid Mech. 164 (1986) 305–336.
[4] D.G. Avraam, A.C. Payatakes, Flow mechanisms, relative permeabilities, and coupling effects in steady-state two-phase flow through porous media. The case of strong wettability, Ind. Eng. Chem. Res. 38 (1999) 778–786.
[5] S.E. Powers, L.M. Abriola, W.J. Weber Jr., An experimental investigation of nonaqueous phase liquid dissolution in saturated subsurface systems: steady state mass transfer rates, Water Resour. Res. 28 (1992) 2691–2705.
[6] A. Mayer, C. Miller, The influence of porous medium characteristics and measurement scale on pore-scale distribution of residual nonaqueous-phase liquids, J. Contam. Hydrol. 11 (1992) 189–213.

[7] A.S. Mayer, C.T. Miller, An experimental investigation of pore-scale distribution of nonaqueous phase liquids at residual saturation, Transport Porous Media 10 (1993) 57–80.
[8] K.D. Pennel, G.A. Pope, L.M. Abriola, Influence of viscous and buoyancy forces on the mobilization of residual tetrachloroethylene during surfactant flushing, Environ. Sci. Technol. 30 (1996) 1328–1335.
[9] N.R. Morrow, Interplay of capillary, viscous and buoyancy forces in the mobilization of residual oil, JNL Can. Petroleum Technol. 18 (1979) 35–46.
[10] J. Chatzis, N.R. Morrow, Correlation of capillary number relationships for sandstone, Soc. Petroleum Eng. J. 24 (5) (1984) 555–562.
[11] F. Gioia, G. Alfani, S. Andreutti, F. Murena, Oil mobility in a saturated water-wetted bed of glass beads, J. Hazard. Mater. B97 (2003) 315–327.
[12] D. Mehta, M.C. Hawley, Wall effects in packed columns, I&EC Proc. Des. Dev. 8 (2) (1969) 280–282.
[13] R.B. Bird, W.E. Stewart, Lightfoot, E.N. Transport Phenomena, John Wiley & Sons, Inc., New York, 1960, p. 200.
[14] A. Gaglione, R. Guida, Mobilizzazione di idrocarburi in mezzi porosi e loro contenimento mediante xanthan gum/Al(III) gel. Tesi di Laurea in Ingegneria Chimica, Università di Napoli Federico II, 2004.
[15] C. Carotenuto, G. Roviello, Simulazione del moto in falde acquifere di oli e loro confinamento mediante la gelled polymer technology, Chemical Engineering Thesis, University of Naples, Italy, 2003.